Z. Phys. A 352, 85 96 (1995)

ZEITSCHRIFT
FÜR PHYSIK A
© Springer-Verlag 1995

Phase-shift analysis of πp scattering in the energy region from 160 to 600 MeV

V.V. Abaev, S.P. Kruglov

Petersburg Nuclear Physics Institute, Gatchina, Leningrad district, 188350, Russia
(Fax: +7-812/71-37196; e-mail: kruglov@lnpi.spb.su.)

Received: 18 April 1994/Revised version: 28 December 1994

Abstract. A phase shift analysis of πN scattering has been carried out at 18 discrete energies in the region 160–600 MeV. Charge splitting of the P_{33} phase shift ($\simeq 2$ degree) is observed with a change of sign at $\simeq 350$ MeV and vanishing at $\simeq 600$ MeV. Marked deviations from an earlier analysis are found for S and P-amplitudes as a result of using new precision data and an untraditional method of the analysis.

PACS: 13.75.G; 14.20

1. Introduction

Recently many πN scattering data for $\sigma(\theta)$, $P(\theta)$, $A(\theta)$ and $R(\theta)$ have been obtained, mostly at LNPI and LAMPF, which should be analysed. The high precision of these data-sets above 300 MeV gives a chance to study the charge splitting of Δ-isobar [1–4] up to 600 MeV. Such "fine" structure needs to take into account Coulomb corrections [5] to the hadronic amplitudes and all inelastic channels, especially for $\pi^- p$ scattering.

The interest to the dynamics of the isospin splitting of the four charge states is based not only on the possibility of the splitting parameters extraction. The strong correlation of the P_{33}-amplitude with other partial waves could be responsible for marked changes for these waves themselves also rather far from the resonance.

Last, the experience obtained in the Δ-isobar region could be fruitful for the analysis of πN scattering in the 1 2 GeV/c region in which we intend to continue our experimental investigations [6] and where possible isospin splitting effects could be more noticeable due to the existence of the well known strong resonance clusters. There are essential disagreements between different analyses there so far [7–9].

2. Procedure of analysis

Owing to the specific character of the goal (investigation of the charge symmetry breaking), we used a slightly modified iteration procedure of a discrete phase shift analysis partly described earlier [10]. Its general scheme is shown below in Fig. 1a.

The block "energy loop" means starting a new discrete phase shift analysis (PSA) at a new energy. When an individual energy T_i is fixed then all available experimental information for the energy T_i will be taken from the block "data-base" to prepare data for the first step "data cleaning" before PSA in the block "$\pi^+ p$ PSA $\pi^- p$". After random PSA (one search) with $l_{max} = 5$ (it means sharp cutting at $L = 5$; for explanation of L-cutting see (Ref. 10)) we obtain one solution and then use this solution as an input for the block "ambiguity generator" to produce all possible solutions (the block "amplitudes"). According to the scheme Fig. 1a, we continue then the PSA with new solutions but in this stage two additional "soft" constraints are imposed on the usual discrete PSA:

1) an isospin $I = 3/2$ constraint which is switched on only in the $\pi^- p$ analysis and enables us to perform it without $\pi^+ p$ data;
2) a high-wave constraint to exclude the necessity of L-cutting.

Isospin $I = 3/2$ "soft" constraints means that adequate amplitudes (phase shifts and inelasticity parameters) are included in the PSA like "experimental" data with some errors. We shall call it "quasi-fixing". The amplitudes with isospin $I = 3/2$ for the $\pi^- p$ analysis are taken from the $\pi^+ p$ analysis with their errors (sometimes amplitudes have to be interpolated to a new energy) and include the whole experimental information on $\pi^+ p$ scattering at the corresponding energy. Any deviations from them during the $\pi^- p$ analysis could be interpreted as indications of an isospin-breaking and have a quantitative measure-the value of χ^2.

The high-wave "soft" constraint deals with the "tails" of small amplitudes ($\delta < 1^\circ$) (phase shifts δ less than 1°)

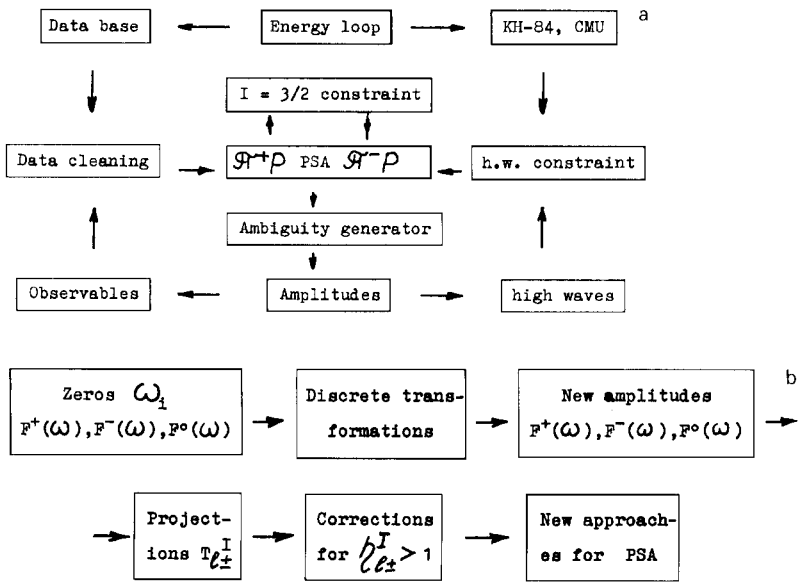

Fig. 1a. The scheme of the phase shift analysis **b)** The scheme of the generator of discrete ambiguities (GDA)

resulting from KH-84 [11], CMU [8] and the first run of our PSA performed without it. Smoothing over energy was done in PSA only in high-wave amplitudes (tails). Interpolated values of these amplitudes were included in the PSA like "experimental" ones, with errors taken from the first run of the PSA or equal to 0.1° in points where they were not determined (limited reachable precision). Inclusion of high-wave constraints allows also to avoid an artificial underestimation of errors in the main principal amplitudes (as was mentioned by D. Bugg [3]) and reach a good agreement with the existing analyses [8, 11] based on the dispersion relations. We have applied this "soft" constraints twice to reach self-consistency.

The block "data cleaning" (Fig. 1a) has two purposes.

First step "data cleaning". If there are two or more identical experiments of different quality at the same energy one needs to exclude the experimental points of the worst quality (from the overlapping angular intervals) to avoid their influence on the high-quality experiment. This influence usually leads to the artificial underestimation of the χ^2 in the PSA. The exclusion is made during the passing data from the data-base to the PSA in the initial stage of the analysis.

Second step "data cleaning". In this step we have to exclude experimental points with large deviations ($\chi^2 > 4$) from smooth angular dependences $\sigma(0)$ and $P(0)$ predicted on the base of the solutions obtained as a result of the PSA. Practically in any experiment one can find one or two points which lie far away from any reasonable smooth curve. The origin could be connected with some unknown systematic error in one of the detection channels. The exclusion of these experimental points leads to an improvement of the χ^2 without visible change of the phase shifts and inelasticity parameters. It is made in the final stage of the analysis.

At some energies a complete data-set is not available. In this case we have to perform an interpolation of data to desirable energy. More often it happens with total cross sections and real parts of the forward amplitudes. This preliminary work is carried out before the analysis and the results are taken to the data-base.

The important part of Fig. 1a is the ambiguity generator or the generator of discrete ambiguities (GDA). Its purpose is to search for all discrete ambiguities of the PSA. GDA is switched on during the last stage of the analysis to produce all possible solutions from known one. These solutions-after applying to them unitarity corrections-are used in the next stage of the analysis. The GDA is described partly in ref. 10, and we shall discuss it more carefully later.

An independent analysis of π^+p scattering at 21 individual energes is the first half of our procedure and is devoted to the extraction of isospin $I = 3/2$ amplitudes. The similar analysis but with L-cutting was reported in earlier paper [10]. Our improved version of it consists of the following stages:

1. Preparation of the π^+p date-base. First step "data cleaning".
2. The PSA at individual energies in the whole energy interval with sharp L-cutting (up to $L = 5$).
3. Search for discrete ambiguities through the GDA at each energy.
4. Continuation of the minimization (PSA) with new solutions.
5. High-wave constraints from the solutions obtained in step 4 and KH-84 and CMU high-wave tails. "Soft" constraint after interpolation of these amplitudes in the whole energy interval. PSA at each individual energy (Right part of Fig. 1a).
6. Second step cleaning the π^+p data and repeatition of paragraph 5 (Left part of Fig. 1a).

The only twofold Barrelet ambiguity is found at 580 MeV and 600 MeV with an acceptable χ^2. The selection of the unique solution is performed on the basis of the criterion of maximum smoothness in both the amplitudes and their Barrelet-zero trajectories (Fig. 1, ref. 10). The obtained solutions for π^+p scattering are considered as

the final ones for isospin $I = 3/2$ and can be used in the $\pi^- p$ analysis like the "soft" constraints.

An attempt to perform an independent $\pi^- p$ analysis leads to incredibly large errors of the amplitudes as a result of the isospin combinations of the $I = 3/2$ and $I = 1/2$-states. To be more objective we have chosen the following way for the analysis:

1. Preparation of the $\pi^- p$ data base. First step "data cleaning". Preparation of the $I = 3/2$-amplitudes from the $\pi^+ p$ analysis for further "soft" constraints (quasi-fixing).
   Sometimes one needs to use an energy interpolation of the data and the amplitudes.
2. PSA at individual energies in the whole energy interval with "soft" $I = 3/2$ constraints and sharp L-cutting (up to $L = 5$) for the amplitudes with isospin $I = 1/2$.
3. Search for discrete ambiguities through the GDA at each energy. Only one solution with an acceptable χ^2 is found.
4. Analysis of the χ^2-map for the isospin $I = 3/2$-amplitudes versus energy. Only the P_{33} amplitude has large systematic deviations from the $\pi^+ p$ channel in the whole energy interval. Other amplitudes have only statistical deviations with a small χ^2.
5. Releasing the P_{33} amplitude from the $I = 3/2$ constraints and repeatition of the PSA at individual energies in the whole energy interval. Reliable P_{33} charge-splitting is observed. No other candidate for visible isospin-splitting is found.
6. Search for the S and P-isospin-mixing amplitudes [12] in the whole energy interval. Only statistical deviations from zero (with a small χ^2) for the isospin-mixing parameters are observed. One can conclude that there are no reliable signals of isospin-mixing.

Table 1. The phase-shifts (in degrees) and the inelasticity parameters for $\pi^+ p$ scattering

T (MeV)	166.0	194.3	236.3	263.6	291.5	309.0	335.0
$\sqrt{S}$ (MeV)	1213.8	1235.5	1267.0	1287.0	1307.2	1319.7	1338.1
S_{31}	-13.46 ± 0.43	-14.96 ± 0.39	-17.87 ± 0.32	-18.52 ± 0.15	-20.37 ± 0.15	-21.72 ± 0.21	-22.49 ± 0.22
	1	1	0.999 ± 0.001	0.998 ± 0.01	0.995 ± 0.001	0.993 ± 0.002	0.993 ± 0.003
P_{33}	71.96 ± 0.32	94.69 ± 0.53	117.50 ± 0.21	126.51 ± 0.12	133.25 ± 0.11	136.50 ± 0.11	140.54 ± 0.15
	1	1	1	1	1	1	1
P_{31}	-4.27 ± 0.52	-4.98 ± 0.45	-6.77 ± 0.43	-7.38 ± 0.22	-8.36 ± 0.21	-8.87 ± 0.26	-9.69 ± 0.39
	1	1	1	1	1	1	0.994 ± 0.004
D_{35}	-0.43 ± 0.09	-0.48 ± 0.14	-0.49 ± 0.14	-0.79 ± 0.20	-0.66 ± 0.19	-1.01 ± 0.24	-0.42 ± 0.24
	1	1	1	1	1	1	1
D_{33}	0.15 ± 0.07	0.21 ± 0.10	0.24 ± 0.10	0.22 ± 0.08	0.26 ± 0.09	0.21 ± 0.09	0.04 ± 0.14
	1	1	1	1	1	1	1
F_{37}	0.08 ± 0.06	0.16 ± 0.08	0.28 ± 0.09	0.33 ± 0.08	0.45 ± 0.08	0.50 ± 0.09	0.52 ± 0.09
	1	1	1	1	1	1	1

T (MeV)	351.6	370.0	399.0	405.0	425.0	446.0	469.0
$\sqrt{S}$ (MeV)	1349.6	1362.4	1382.2	1386.3	1399.7	1413.8	1428.7
S_{31}	-23.90 ± 0.24	-24.77 ± 0.40	-25.28 ± 0.33	-25.07 ± 0.33	-26.63 ± 0.32	-26.21 ± 0.54	-25.54 ± 0.40
	0.992 ± 0.003	0.991 ± 0.003	0.990 ± 0.004	0.989 ± 0.004	0.989 ± 0.003	0.988 ± 0.004	0.985 ± 0.005
P_{33}	142.89 ± 0.15	144.98 ± 0.23	147.91 ± 0.23	148.18 ± 0.23	150.16 ± 0.22	151.74 ± 0.34	153.41 ± 0.29
	1	1	1	1	1	1	1
P_{31}	-10.04 ± 0.31	-10.19 ± 0.51	-12.14 ± 0.48	-12.09 ± 0.48	-11.76 ± 0.46	-12.03 ± 0.75	-12.28 ± 0.62
	0.991 ± 0.004	0.988 ± 0.005	0.986 ± 0.008	0.988 ± 0.008	0.966 ± 0.006	0.965 ± 0.009	0.948 ± 0.010
D_{35}	-1.13 ± 0.23	-0.95 ± 0.31	-1.18 ± 0.35	-1.13 ± 0.35	-1.80 ± 0.36	-1.63 ± 0.60	-2.35 ± 0.41
	1	1	1	1	1	1	1
D_{33}	-0.06 ± 0.23	-0.14 ± 0.28	-0.22 ± 0.32	-0.16 ± 0.31	0.63 ± 0.33	0.14 ± 0.50	0.41 ± 0.50
	1	1	0.998 ± 0.002	0.997 ± 0.002	0.996 ± 0.002	0.995 ± 0.003	0.993 ± 0.003
F_{37}	0.76 ± 0.09	0.76 ± 0.09	0.86 ± 0.09	0.90 ± 0.09	1.05 ± 0.17	1.06 ± 0.23	1.52 ± 0.17
	1	1	1	1	1	1	1

T (MeV)	490.0	500.8	510.0	531.0	560.0	581.0	599.0
$\sqrt{S}$ (MeV)	1442.7	1449.7	1455.6	1469.1	1487.5	1500.7	1511.9
S_{31}	-26.54 ± 0.41	-27.35 ± 0.36	-27.75 ± 0.40	-27.94 ± 0.30	-27.51 ± 0.28	-27.93 ± 0.32	-27.45 ± 0.37
	0.982 ± 0.004	0.975 ± 0.007	0.970 ± 0.008	0.953 ± 0.010	0.930 ± 0.010	0.910 ± 0.013	0.883 ± 0.015
P_{33}	155.05 ± 0.29	156.67 ± 0.26	157.75 ± 0.41	159.40 ± 0.34	161.37 ± 0.38	163.47 ± 0.54	164.56 ± 0.52
	0.994 ± 0.006	0.991 ± 0.007	0.983 ± 0.006	0.990 ± 0.006	0.970 ± 0.006	0.967 ± 0.007	0.956 ± 0.008
P_{31}	-11.75 ± 0.62	-12.91 ± 0.46	-13.07 ± 0.94	-13.21 ± 0.86	-12.87 ± 0.95	-15.61 ± 1.45	-15.31 ± 1.26
	0.950 ± 0.007	0.948 ± 0.011	0.963 ± 0.007	0.954 ± 0.008	0.962 ± 0.006	0.959 ± 0.008	0.962 ± 0.009
D_{35}	-3.05 ± 0.39	-2.87 ± 0.28	-3.45 ± 0.45	-3.43 ± 0.40	-3.80 ± 0.45	-3.28 ± 0.59	-3.60 ± 0.51
	1	1	1	1	1	1	1
D_{33}	1.61 ± 0.37	1.62 ± 0.33	2.50 ± 0.47	2.39 ± 0.44	2.41 ± 0.48	1.50 ± 0.69	1.49 ± 0.58
	0.990 ± 0.004	0.989 ± 0.05	0.986 ± 0.006	0.973 ± 0.006	0.967 ± 0.006	0.957 ± 0.006	0.941 ± 0.008
F_{37}	1.57 ± 0.18	1.72 ± 0.13	1.46 ± 0.18	1.57 ± 0.17	1.82 ± 0.15	2.32 ± 0.19	2.60 ± 0.19
	1	1	1	1	1	1	1

Table 2. The phase-shifts (in degrees) and the inelasticity parameters for $\pi^- p$ scattering

T (MeV)	161.9	237.9	263.6	290.0	309.0	335.0
$\sqrt{S}$ (MeV)	1210.6	1268.1	1287.0	1306.1	1319.7	1338.1
S_{31}	-13.08 ± 0.49	-17.87 ± 0.28	-18.53 ± 0.15	-20.47 ± 0.15	-21.74 ± 0.20	-22.50 ± 0.22
	1	0.999 ± 0.001	0.998 ± 0.001	0.995 ± 0.001	0.993 ± 0.002	0.992 ± 0.003
S_{11}	10.02 ± 0.36	10.66 ± 0.38	11.31 ± 0.27	11.43 ± 0.27	11.88 ± 0.47	12.66 ± 0.44
	1	1	1	1	1	1
P_{33}	66.21 ± 0.30	115.92 ± 0.39	124.35 ± 0.29	131.30 ± 0.33	135.39 ± 0.48	139.50 ± 0.66
	1	1	1	1	1	1
P_{13}	-1.62 ± 0.30	-3.14 ± 0.29	-3.27 ± 0.23	-3.59 ± 0.21	-3.15 ± 0.41	-3.42 ± 0.52
	1	1	1	1	1	1
P_{31}	-4.27 ± 0.52	-6.44 ± 0.33	-7.34 ± 0.22	-8.22 ± 0.19	-8.94 ± 0.23	-9.71 ± 0.36
	1	1	1	1	1	0.994 ± 0.004
P_{11}	0.60 ± 0.52	5.99 ± 0.30	9.24 ± 0.34	13.22 ± 0.33	17.97 ± 0.47	23.75 ± 0.81
	0.997 ± 0.001	0.996 ± 0.002	0.985 ± 0.008	0.975 ± 0.008	0.935 ± 0.011	0.868 ± 0.016
D_{35}	-0.43 ± 0.10	-0.45 ± 0.13	-0.74 ± 0.20	-0.45 ± 0.16	-1.19 ± 0.20	-0.55 ± 0.21
	1	1	1	1	1	1
D_{15}	0.41 ± 0.19	1.05 ± 0.24	1.34 ± 0.21	1.72 ± 0.16	1.98 ± 0.19	2.16 ± 0.22
	1	1	1	1	1	1
D_{33}	0.15 ± 0.07	0.21 ± 0.10	0.21 ± 0.10	0.26 ± 0.10	0.15 ± 0.10	0.01 ± 0.14
	1	1	1	1	1	1
D_{13}	0.53 ± 0.18	1.76 ± 0.21	2.39 ± 0.19	3.41 ± 0.20	4.40 ± 0.25	5.03 ± 0.33
	1	1	0.999 ± 0.004	0.989 ± 0.004	0.990 ± 0.005	0.988 ± 0.007

T (MeV)	351.6	370.0	389.0	425.0	446.0	463.0
$\sqrt{S}$ (MeV)	1349.6	1362.4	1375.4	1399.7	1413.8	1425.0
S_{31}	-23.87 ± 0.23	-24.76 ± 0.36	-25.38 ± 0.36	-26.44 ± 0.30	-26.04 ± 0.49	-25.61 ± 0.38
	0.993 ± 0.003	0.991 ± 0.003	0.990 ± 0.004	0.989 ± 0.003	0.988 ± 0.004	0.985 ± 0.005
S_{11}	12.88 ± 0.48	13.73 ± 0.53	14.34 ± 0.86	15.53 ± 0.82	17.54 ± 1.15	18.72 ± 1.27
	1	1	1	1	1	1
P_{33}	143.12 ± 0.35	145.67 ± 0.64	147.92 ± 0.86	151.87 ± 0.65	153.19 ± 0.83	155.14 ± 0.84
	1	1	1	1	1	1
P_{13}	-4.40 ± 0.25	-3.99 ± 0.51	-3.98 ± 0.50	-4.81 ± 0.53	-5.20 ± 0.77	-5.12 ± 0.80
	1	1	1	0.984 ± 0.018	0.961 ± 0.022	0.951 ± 0.023
P_{31}	-10.06 ± 0.29	-10.20 ± 0.50	-11.16 ± 0.49	-12.07 ± 0.43	-12.23 ± 0.69	-12.43 ± 0.56
	0.991 ± 0.004	0.989 ± 0.004	0.987 ± 0.005	0.965 ± 0.006	0.964 ± 0.008	0.951 ± 0.009
P_{11}	27.35 ± 0.52	32.24 ± 1.04	37.10 ± 1.16	44.53 ± 0.97	49.98 ± 1.84	55.66 ± 2.15
	0.835 ± 0.012	0.735 ± 0.022	0.663 ± 0.024	0.559 ± 0.026	0.487 ± 0.031	0.482 ± 0.036
D_{35}	-1.16 ± 0.21	-1.30 ± 0.28	-1.11 ± 0.31	-1.72 ± 0.27	-1.75 ± 0.41	-2.04 ± 0.34
	1	1	1	1	1	1
D_{15}	2.55 ± 0.19	2.38 ± 0.27	2.94 ± 0.34	3.41 ± 0.26	3.70 ± 0.35	3.79 ± 0.34
	1	1	1	1	1	1
D_{33}	-0.15 ± 0.22	-0.38 ± 0.27	-0.21 ± 0.29	0.05 ± 0.30	-0.20 ± 0.43	0.64 ± 0.44
	1	1	1	0.996 ± 0.002	0.995 ± 0.003	0.993 ± 0.003
D_{13}	6.73 ± 0.22	7.27 ± 0.33	8.67 ± 0.36	12.08 ± 0.33	13.90 ± 0.48	16.15 ± 0.50
	0.972 ± 0.005	0.970 ± 0.009	0.961 ± 0.008	0.927 ± 0.012	0.925 ± 0.016	0.914 ± 0.016

T (MeV)	490.0	500.8	531.5	560.7	571.8	599.0
$\sqrt{S}$ (MeV)	1442.7	1449.7	1469.4	1487.9	1494.9	1511.9
S_{31}	-26.31 ± 0.39	-27.57 ± 0.33	-27.87 ± 0.29	-27.42 ± 0.27	-27.70 ± 0.30	-27.43 ± 0.36
	0.982 ± 0.004	0.975 ± 0.006	0.952 ± 0.009	0.930 ± 0.010	0.919 ± 0.012	0.878 ± 0.015
S_{11}	20.95 ± 0.79	20.49 ± 0.77	25.85 ± 0.97	35.64 ± 1.05	41.29 ± 3.31	43.08 ± 2.44
	1	1	1	0.887 ± 0.024	0.777 ± 0.037	0.552 ± 0.033
P_{33}	157.56 ± 0.72	157.84 ± 0.68	160.25 ± 0.69	161.67 ± 0.60	163.16 ± 1.06	165.68 ± 0.93
	0.996 ± 0.004	0.991 ± 0.006	0.992 ± 0.005	0.972 ± 0.005	0.971 ± 0.007	0.959 ± 0.007
P_{13}	-5.07 ± 0.70	-5.99 ± 0.58	-5.38 ± 0.66	-5.42 ± 0.68	-6.87 ± 1.49	-8.55 ± 0.93
	0.910 ± 0.020	0.922 ± 0.019	0.910 ± 0.024	0.896 ± 0.023	0.872 ± 0.029	0.860 ± 0.026
P_{31}	-13.34 ± 0.55	-12.75 ± 0.41	-13.87 ± 0.63	-13.63 ± 0.68	-14.52 ± 1.07	-16.29 ± 1.13
	0.949 ± 0.007	0.951 ± 0.010	0.951 ± 0.008	0.962 ± 0.006	$0.961 \pm .007$	0.963 ± 0.008
P_{11}	62.16 ± 1.85	63.18 ± 1.58	71.04 ± 1.62	88.26 ± 3.12	90.54 ± 5.15	106.08 ± 4.87
	0.423 ± 0.026	0.430 ± 0.025	0.356 ± 0.026	0.351 ± 0.024	0.343 ± 0.032	0.350 ± 0.037
D_{35}	-3.10 ± 0.32	-3.19 ± 0.23	-3.46 ± 0.31	-3.27 ± 0.32	-2.66 ± 0.44	-3.35 ± 0.44
	1	1	1	1	1	1
D_{15}	4.04 ± 0.33	4.72 ± 0.23	4.68 ± 0.26	6.17 ± 0.30	6.30 ± 0.51	7.12 ± 0.64
	1	1	1	1	1	1
D_{33}	1.40 ± 0.33	1.53 ± 0.28	2.04 ± 0.36	2.02 ± 0.39	2.18 ± 0.55	1.68 ± 0.50
	0.990 ± 0.004	0.989 ± 0.005	0.972 ± 0.006	0.968 ± 0.006	0.962 ± 0.007	0.939 ± 0.008
D_{13}	18.82 ± 0.60	21.02 ± 0.51	29.80 ± 0.76	38.62 ± 0.86	41.60 ± 1.88	65.60 ± 4.38
	0.893 ± 0.014	0.847 ± 0.016	0.760 ± 0.023	0.601 ± 0.022	0.528 ± 0.043	0.212 ± 0.034

7. High-wave constraints from the obtained $I = 1/2$ solutions and KH-84 and CMU high-wave tails. PSA with "soft" constraints at each individual energy. (Right part of Fig. 1a).
8. Second step cleaning $\pi^- p$ data and repeatition of item 7 (Left part of Fig. 1a).

The obtained amplitudes with isospin $I = 1/2$ are considered like final ones. The second set of the $I = 3/2$ amplitudes coincides with the first one (from the $\pi^+ p$ analysis) within the errors, except the P_{33} phase shifts (charge-splitting).

The GDA [10] is based on the Barrelet formalism [13, 14]. The transformations responsible for discrete ambiguities could be non-unitary in a common case. Therefore the block-scheme of the GDA has to be like presented in Fig. 1b where $F^+(\omega)$ $F^+(\omega)$ and $F^0(\omega)$ are the transversity amplitudes of the reactions $\pi^+ p \to \pi^+ p$, $\pi^- p \to \pi^- p$, and $\pi^- p \to \pi^0 n$. The transformations invariant for any observable, except the spin-rotation parameters, are generated by any even combinations of the Minami Yang transformations and the Barrelet transformations. Their simplest representation is expressed in terms of the transversity amplitude zeros ω_i [10].
For the $\pi^+ p$ scattering we have the following steps:

1. After performing PSA one needs to find the zeros ω_i of $F^+(\omega)$-amplitude.
2. Perform the discrete transformations:
   Any combinations of the Minami Yang transformations

   $F^+(\omega) = \omega^n F^+(\omega), \quad n = \pm 1, \pm 2, \ldots ;$

   Barrelet conjugations (2^{2L}-solutions): $\omega_i \to 1/\omega_i^*$.
3. Projection of the new amplitude $F^+(\omega)$ on the partial-wave amplitudes $T_{l\pm}^{3/2}$.
4. Analysis of all inelasticity parameters for unitarity ($\eta_l^{3/2} \leqslant 1$) and correction of non-unitary solutions ($\eta_{l\pm}^{3/2} \geqslant 1 + \Delta\eta$) to the unitary limit ($\eta_{l\pm}^{3/2} = 1$). The tuning parameter $\Delta\eta$ is chosen to be 0.03. Attempts to continue PSA from solutions with $\Delta\eta > 0.03$ lead to very bad χ^2 or to disappearance of the minimum.
5. Placing all new solutions in memory for further stages of the analysis.

For the $\pi^- p$ scattering there are some specific features:

1. Searching for zeros of the amplitudes $F^-(\omega)$ and $F^0(\omega)$.
2. Discrete transformations for both amplitudes. Two times more solutions are obtained.
3. Partial-wave projections on isospin combinations of each channel. Subtraction of the $I = 3/2$-amplitudes (they are known from the initial solution) and production of the $I = 1/2$-amplitudes.
   It is important to notice that some transformations invariant for one channel could be non-invariant for another one. The minimum structure in the partial-wave space is not so trivial as for $\pi^+ p$ scattering.
4. Unitarity correction of the $I = 1/2$-amplitudes in all solutions.
5. Placing all solutions with new $I = 1/2$-amplitudes and old $I = 3/2$-amplitudes in memory for further stages of the analysis.

3. Results

The phase shift analysis is performed at 21 energies for $\pi^+ p$ scattering and at 18 energies for $\pi^- p$ scattering in the energy range from 162 to 600 MeV.

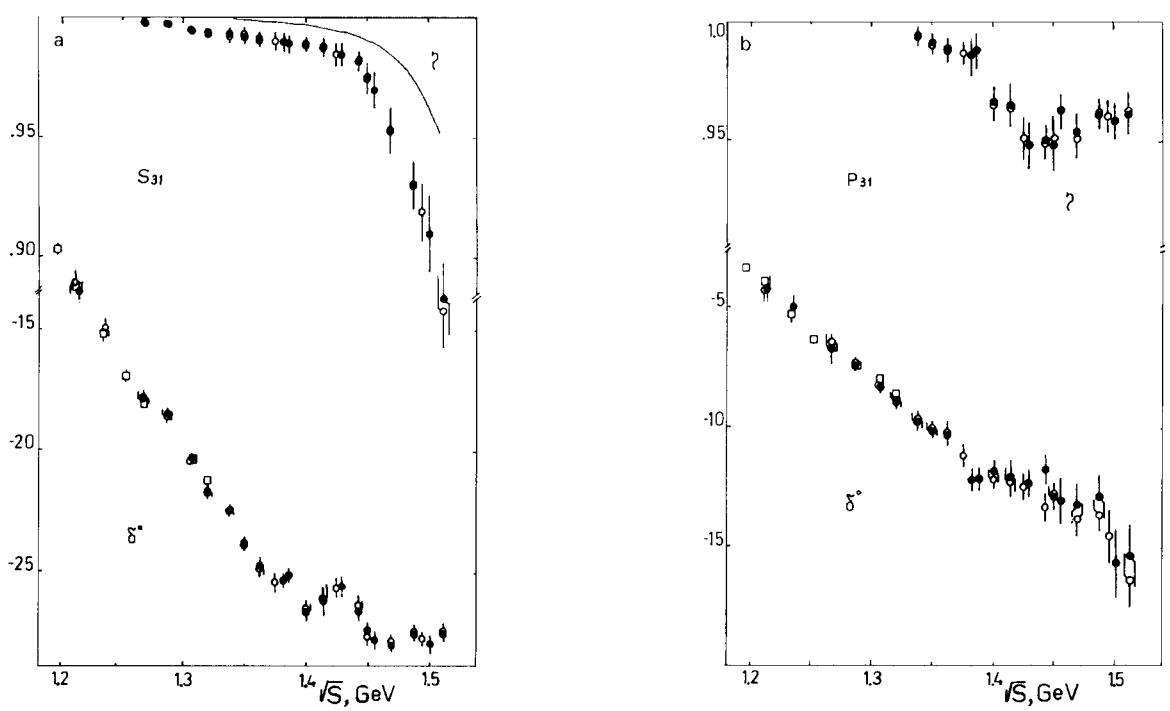

Fig. 2. (continued)

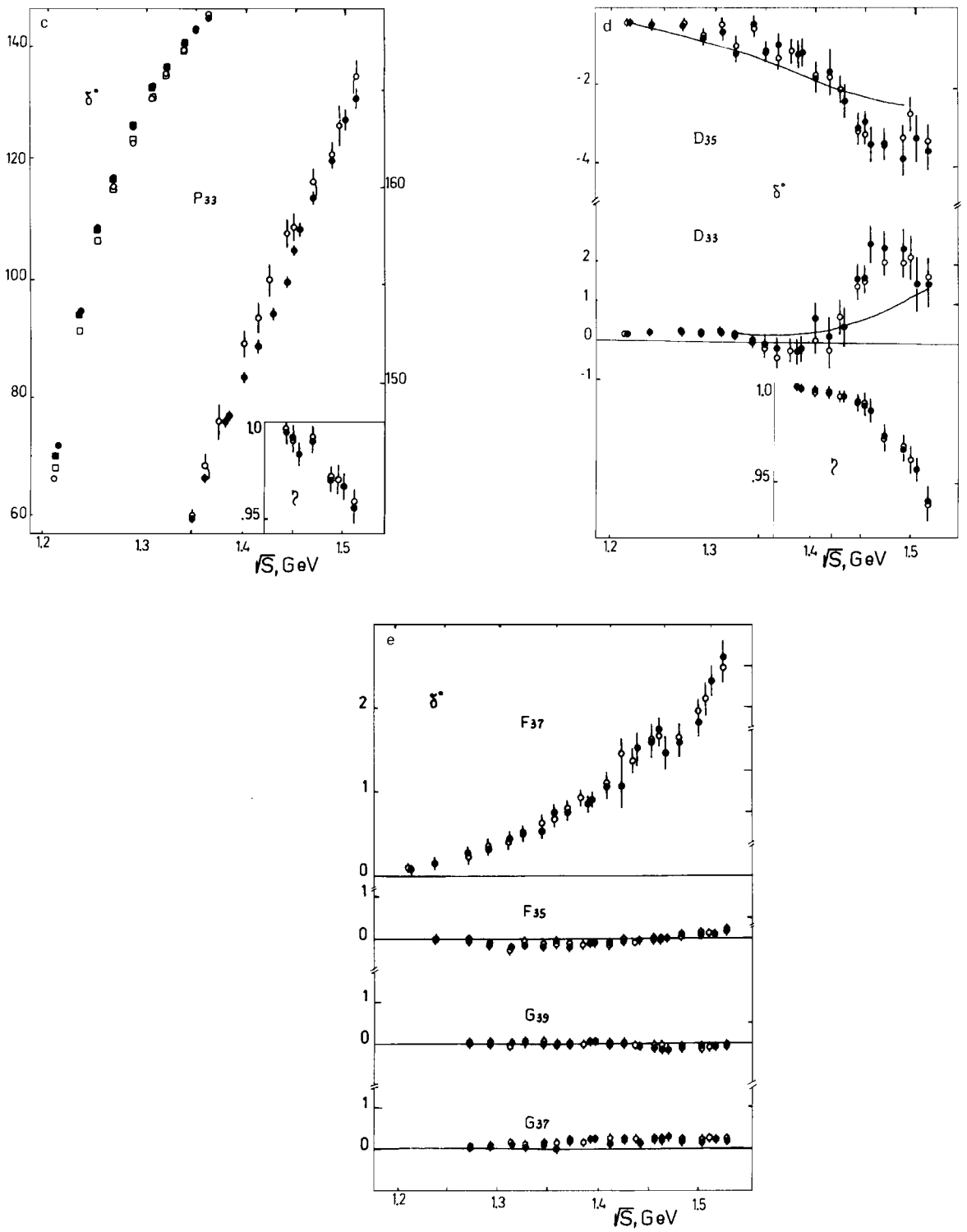

Fig. 2a–e. The phase shifts $\delta_{I\,l}$ and inelasticity parameters η for isospin $I = 3/2$ obtained in this work from the $\pi^+ p$ analysis (●) and from the $\pi^- p$ analysis (○). Also presented are the phase shifts from D. Bugg analysis (□) and KH-84 (curve), **c–e** the same as Fig. 2a

The description of the experimental data with complete information (χ^2 per one experimental point; χ^2 per number of the freedom degrees; χ^2 per one experimental point for each observable; excluded experimental points; scale parameters; confidence level) is given in Ref. [15]. We have used the most precise data on $\sigma(\theta)$, $P(\theta)$, $A(\theta)$ and $R(\theta)$ [20 61].

The total cross sections are taken as a result of an interpolation of the data [16], real parts of the forward amplitude from [17], the total elastic cross sections-from [18, 20 22], the total inelastic cross sections-from the compilation [19] of the reactions: $\pi^+ p \to \pi^+ \pi^0 p$, $\pi^+ \pi^+ n$ and $\pi^- p \to \gamma n$, $\pi^- \pi^0 p$, $\pi^+ \pi^- n$, $\pi^0 \pi^0 n$, ηn.

The results of the analysis are given in Tables 1 and 2 for $\pi^+ p$ and $\pi^- p$ scattering, respectively. Both Tables contain the amplitudes with isospin $I = 3/2$, but for $\pi^- p$ scattering they are considered like the quasi-fixed ones ("soft" $I = 3/2$-constraints) from $\pi^+ p$ scattering (from Table 1), except the P_{33} amplitude. There is good agreement between both sets. Only for the P_{33} phase shifts two different solutions exist. We interpret it as the charge-splitting.

The same results are shown in Figs. 2 and 3 in comparison with KH-84 (solid curves) and Bugg's results [3]. The curves are given only in some pictures where the largest discrepancy exists. Bugg's analysis is performed up to the total energy $W = \sqrt{s} = 1.32$ GeV and its results are shown to demonstrate good agreement including the P_{33} amplitude. One needs to notice that Bugg's errors are underestimated due to the "freezing" of the high-wave tails as he mentions himself [3].

Figure 4 demonstrates deviations of the P_{33} phase shifts from an interpolated curve for the P_{33} phase shifts KH-80 [7] and Koch's [62] analysis ($\Delta\delta = \delta$ (PNPI)-δ (KH)). This representation is more suitable to show the slight deviations from the smooth interpolated curve with a large derivative.

The pure charge-splitting effect of the P_{33} phase shifts ($\delta^{++} - \delta^0$, degrees) is shown in the same Figure in comparison with Bugg's results [3]. There is good agreement in the overlapping energy interval.

The amplitude's errors for the $\pi^- p$ scattering are two or three times larger than the amplitude's errors for the $\pi^+ p$ scattering (Fig. 4). The main reason is a lack of high quality data on charge-exchange differential cross sections. We plan to perform these measurements at PNPI in the region W from 1.35 GeV to 1.5 GeV.

The most interesting results of this analysis are the following:

1. The value of the charge-splitting for the P_{33} phase shifts ($\delta^{++} - \delta^0$) depends on energy, changing sign at $W \simeq 1.35$ GeV and vanishing at $W \simeq 1.5$ GeV (Fig. 4).
2. A systematic deviation of the S_{11} phase shift and the inelasticity parameters of the S_{31} amplitude from KH-84 (Fig. 3a, 2a).
3. Large inelasticity in the P_{31} and P_{13} amplitudes (Fig. 2b, 3c), lacking for KH-84 ($\eta = 1$).
4. Marked deviations of the D_{35}, D_{33}, and D_{15} phase shifts from the results of KH-84 (Fig. 2d, 2e, 3e).

The Argand plots, real (Re) and imaginary (Im) parts and derivatives of the most interesting amplitudes are shown in Figs. 5–8. The derivatives of the amplitudes $T'_{l\pm}(W)$ were calculated using the formula:

$$|T'_{l\pm}(W)| = 0.5\sqrt{(\eta'_{l\pm})^2 + (2\eta_{l\pm}\delta'_{l\pm})^2}$$

where $\delta'_{l\pm}(W)$ and $\eta'_{l\pm}(W)$ are the derivatives of the phase shifts and inelasticity parameters at the total energy W. The normalisation of the derivatives of the amplitudes $|T'_{l\pm}|$ in Figs. 5 to 8 is arbitrary since only the position of maximum has physical meaning. For convenience the derivatives are normalized to unity in their own maximum (including errors).

To calculate the derivatives one needs to perform some energy interpolation of the phase shifts and inelasticity parameters. To be model-independent, we have decided to take the average value of two methods of linear interpolation:

1. Average of right and left derivatives with weights:

$$\left(1 - \frac{\Delta W_r}{\Delta W}\right), \left(1 - \frac{\Delta W_l}{\Delta W}\right),$$

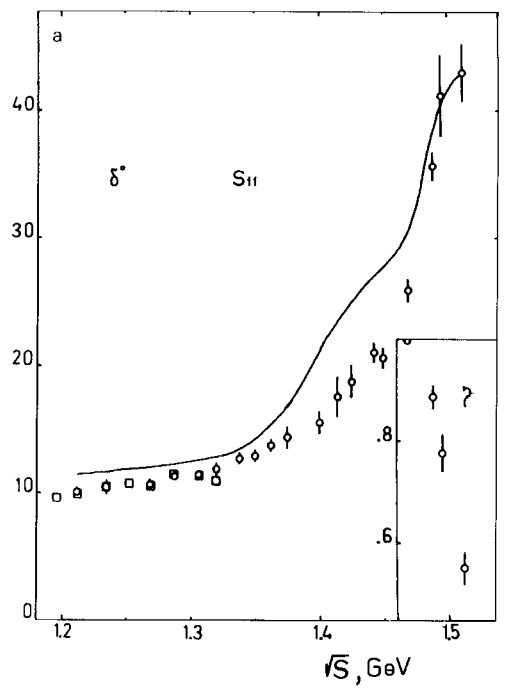

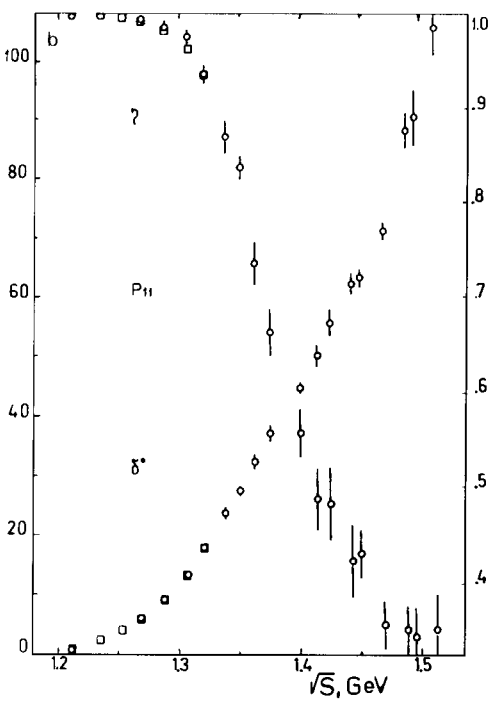

Fig. 3. (continued)

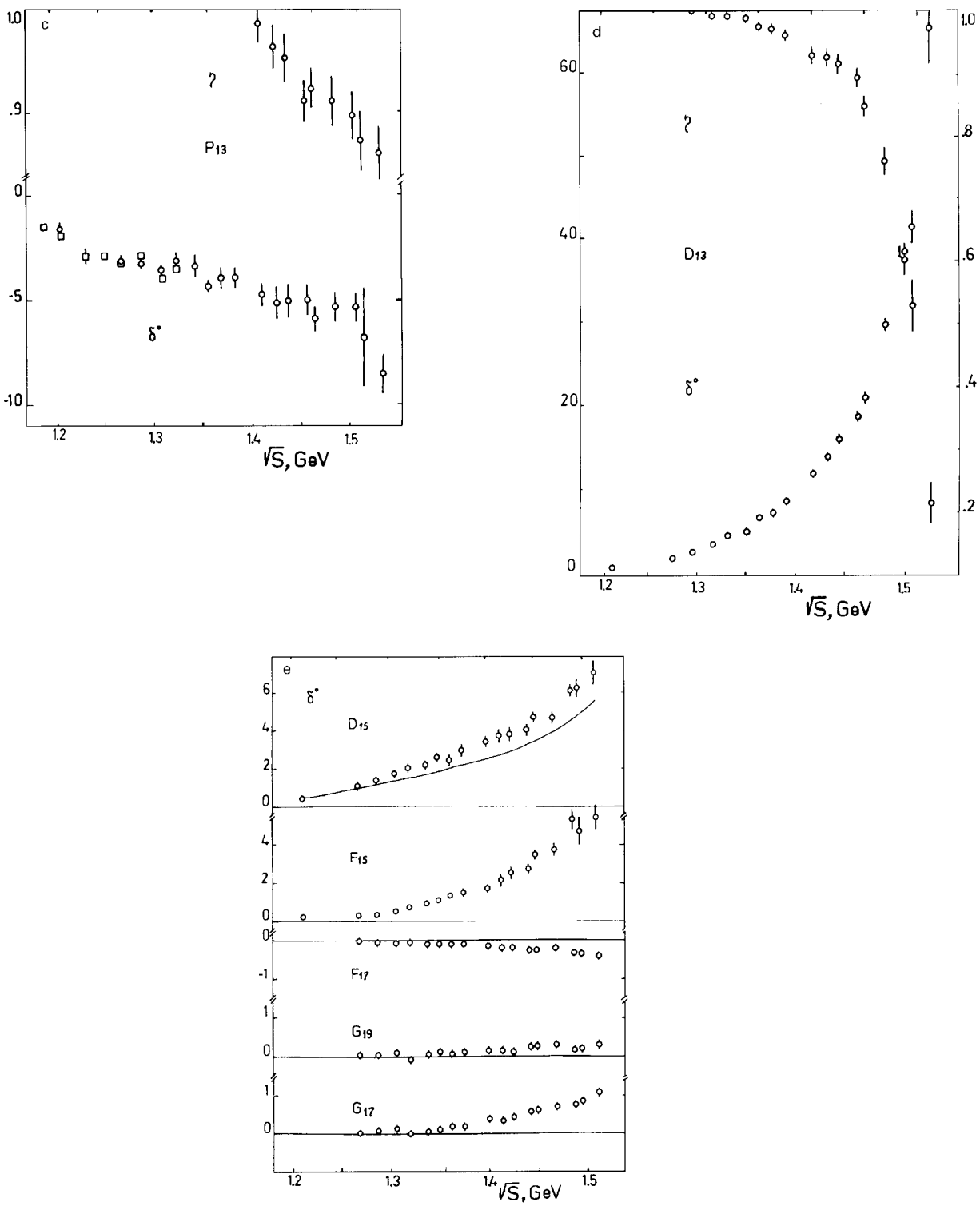

Fig. 3a–e. The phase shifts $\delta_{l\pm}$ and inelasticity parameters η for isospin $I = 1/2$ obtained in this work from the $\pi^- p$ analysis (○). Also presented are the phase shifts from D. Bugg analysis (□) and KH-84 (*curve*)

where $\Delta W_r = W_r - W$, $\Delta W_l = W_l - W$, $\Delta W = W_r - W_l$ and $W_{r,l}$ are right and left energies. The nearer the near-by point, the bigger its weight.

2. Average of right and left derivatives with weights:

$$\left(1 - \frac{\Delta_r}{\Delta}\right), \left(1 - \frac{\Delta_l}{\Delta}\right),$$

where $\Delta_r + \Delta_l$ – errors in the right and the left points, $\Delta = \Delta_r + \Delta_l$. The less the error in the near-by point, the bigger its weight.

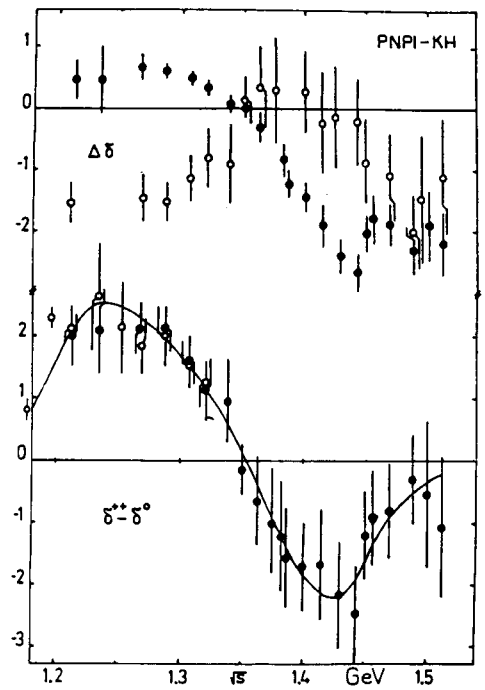

Fig. 4. Charge splittings of P_{33} phase shifts (degrees). *Top plot*: $\Delta\delta = \delta$ (PNPI) $- \delta$ (KH); ● $\pi^+ p$ scattering, ○ $\pi^- p$ scattering *Bottom plot*: $\delta^{++} - \delta^0$; ● present analysis, ○ D.Bugg analysis, *solid curve* result of calculations (see text)

The derivatives at the edge points are calculated only from one nearest point and are not so reliable.

In accordance with the resonance criteria, the amplitudes P_{33}, P_{11}, S_{11} and D_{13} have resonances. The extraction of the S_{11} and D_{13}-resonance parameters is not possible because their right wings are lying outside the region of the analysis. The derivative of the S_{11}-amplitude has a strong narrow peak at $W = 1487$ MeV due to the threshold of the reaction $\pi^- p \to \eta n$.

For the P_{11} amplitude all criteria, except the maximum of the derivative, indicate the resonance mass at $W \simeq 1470$ MeV. But the derivative has a maximum at $W \simeq 1350$ MeV. In papers [63, 64], it is predicted that there is a strong background in this amplitude which describes it at low energies and has a large derivative. Therefore, an extraction of the P_{11}-resonance parameters requires a special investigation.

The parametrization of the P_{33} phase shifts (δ^{++} and δ^0) proved to be model-dependent for the resonance and background terms. Our calculations are performed with the relativistic Breit–Wigner resonance term [65] and with the background $\delta_b\,(q) = q^3\ \Pi\ (q - q_i)$, where q is c.m. moment and q_1 is momentum in the resonance ($W = M$). The background is equal to zero in the resonance ($q = q_1$).

We have taken into account Bugg's data [3] up to 300 MeV and described the specific energy behaviour of $\delta^{++} - \delta^0$ (solid curve on Fig. 4) with the following resonance parameters (MeV):

M^{++}	M^0	$M^0 - M^{++}$	$\Gamma^0 - \Gamma^{++}$
1230.5 ± 0.2	1233.1 ± 0.3	2.6 ± 0.4	5.1 ± 1.0

The widths are not given because they are the most model-dependent values. The energy dependence of the charge-splitting $\delta^{++} - \delta^0$ is confirmed in a model calculation at low energies [66].

In Figs. 9 and 10 one can see the description of very difficult experiments on measurement of the spin-rotation parameters in πp scattering performed at LAMPF [23] and LNPI [24]. The agreement is good.

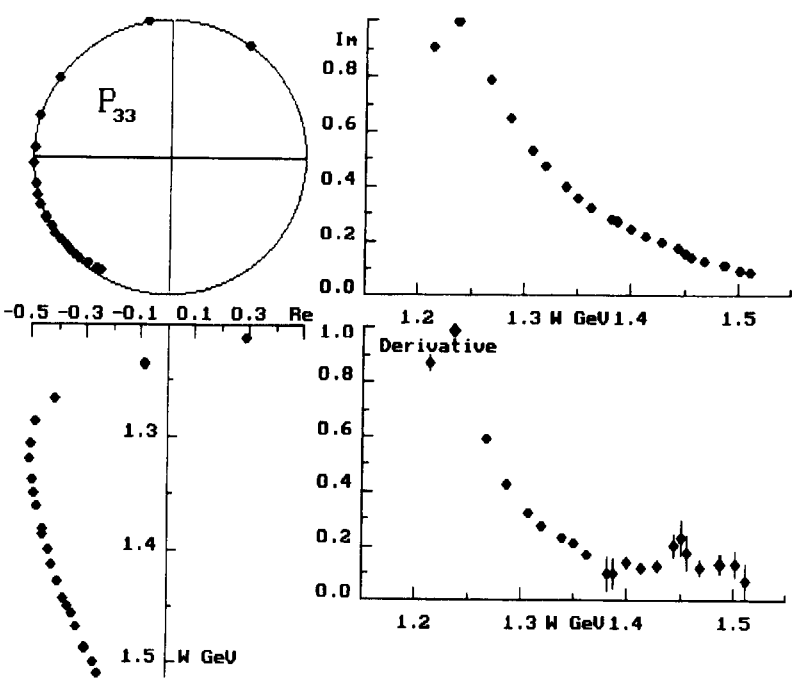

Fig. 5. The Argand plot, real and imaginary parts and derivative of the P_{33} amplitude

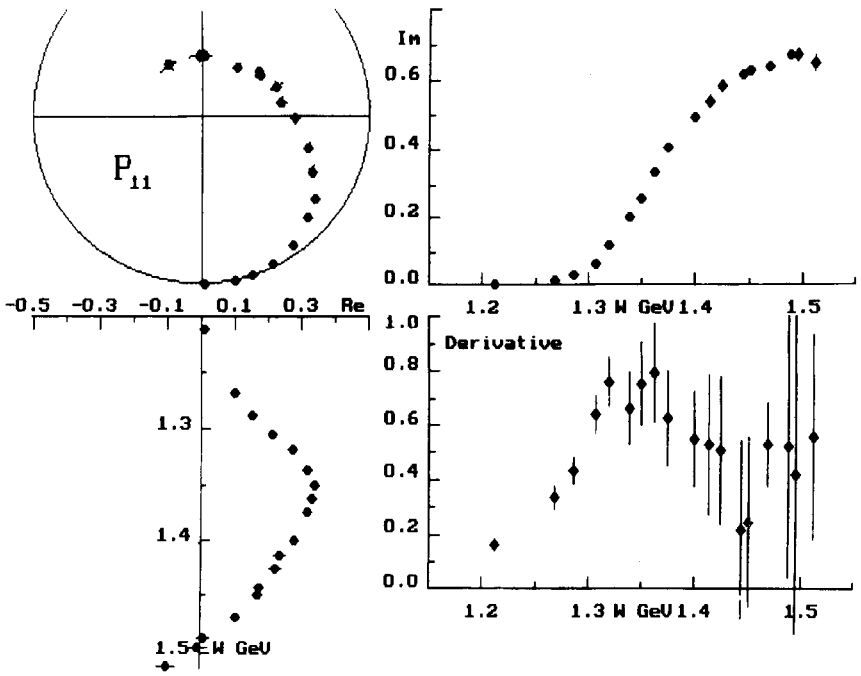

Fig. 6. The Argand plot, real and imaginary parts and derivative of the P_{11} amplitude

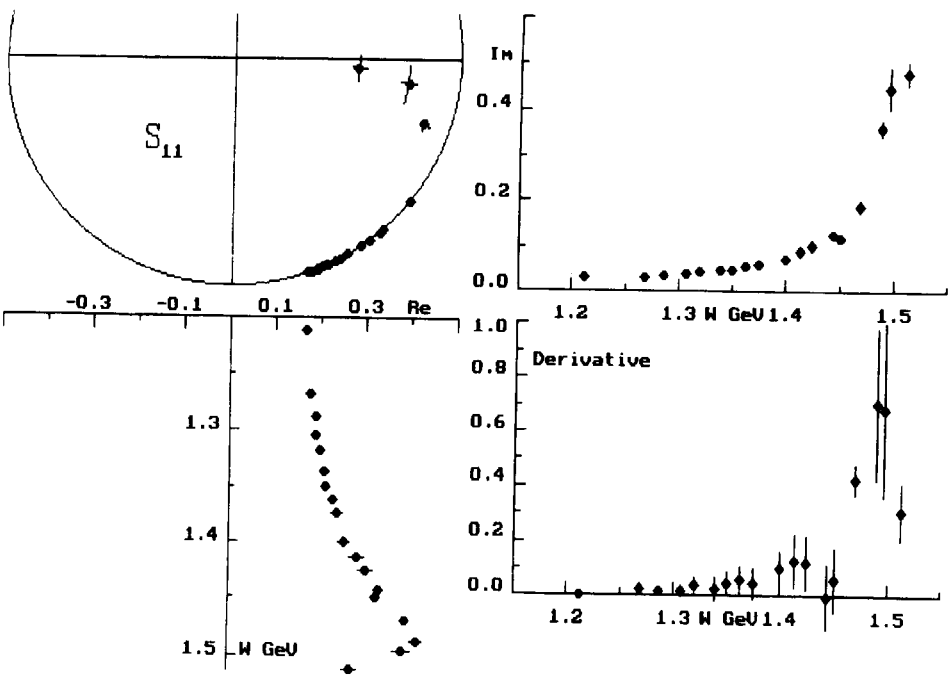

Fig. 7. The Argand plot, real and imaginary parts and derivative of the S_{11} amplitude

The authors are grateful to B. Nefkens and M. Sadler for their data on the spin-rotation parameters kindly proposed to be taken into consideration, and G. Hohler, D. Cutkosky, D. Bugg, J. Stachov, F. Nichitiu, A. Gridnev, I. Lopatin for interesting and fruitful discussions. This work is supported in part by Russian Foundation for Fundamental Research.

References

1. Carter J.R. et al., Nucl. Phys. B58, 378 (1973).
2. Alder J.C. et al., Phys. Rev. D27, 1040 (1983).
3. Bugg D.V., πN Newsletter 6 (1992), 7, ed R.E. Cutkosky, G. Hohler, W. Kluge and B. M. K. Nefkens.
4. Abaev V.V., Proc. of the 3rd Int. Symp. "Pion-Nucleon and Nucleon-Nucleon Interactions", Gatchina, 147 (1989).
5. Tromborg B. et al., Phys. Rev. D15, 725 (1977); Helv. Phys. Acta 51, 584 (1978).
6. Abaev V.V. et al., Preprint ITEP 34 90 (1990).
7. Hohler G., Pion-nucleon scattering, in Landolt-Bornstein Schopper, H. (ed.), Vol. I/9b, Parts 1 and 2, Berlin, Heidelberg, New York: Springer 1983.
8. Cutkosky R.E. et al., Phys. Rev. D20, 2839 (1979).
9. Arndt R.A. et al., Phys. Rev. Lett. 65, 157 (1990).

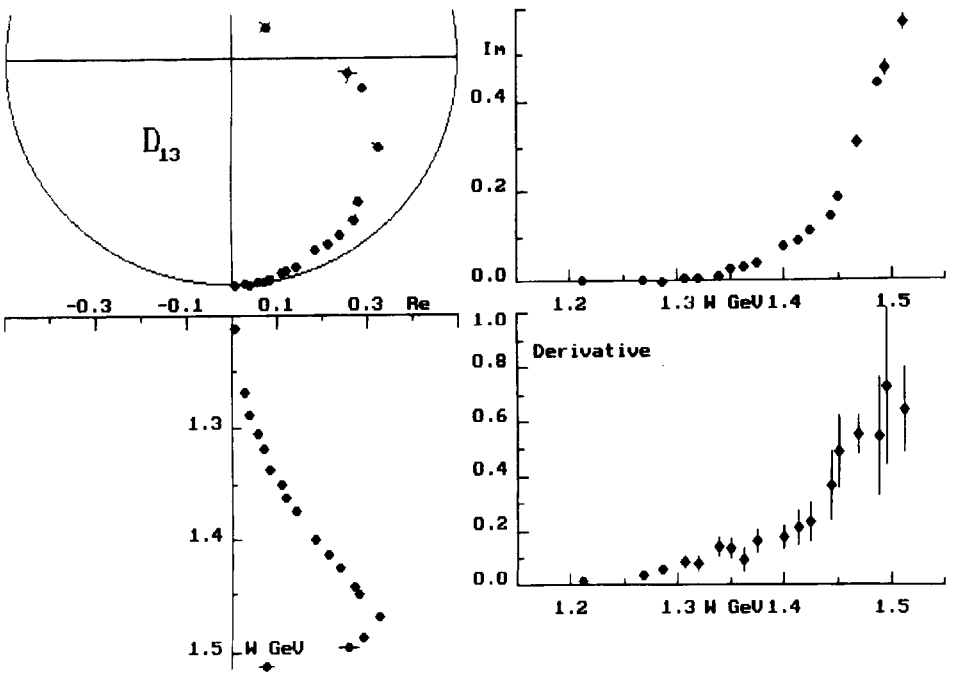

Fig. 8. The Argand plot, real and imaginary parts and derivative of the D_{13} amplitude

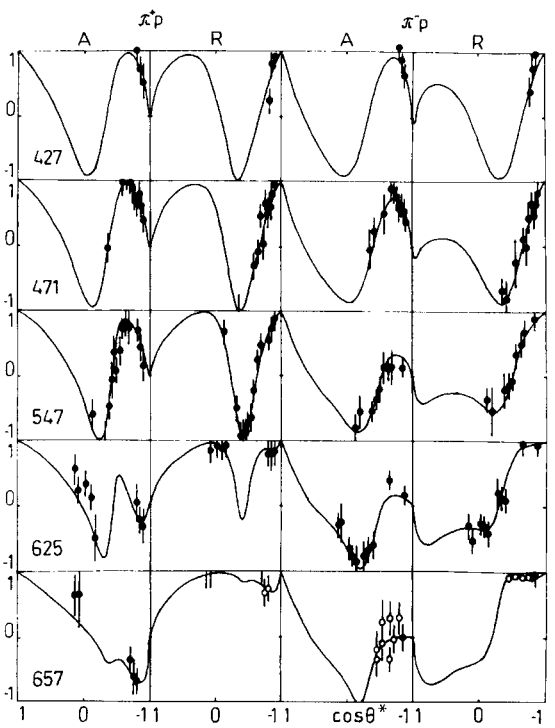

Fig. 9. The spin-rotation parameters. ● reference [20]; ○ reference [21]; momentum in MeV/c

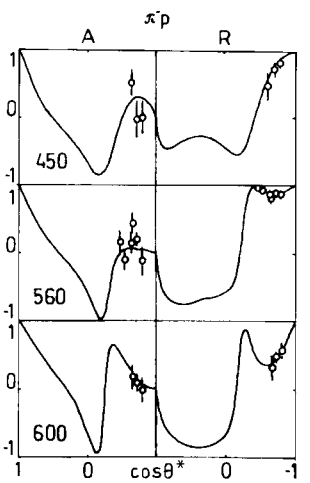

Fig. 10. The spin-rotation parameters ○ reference [21]; energy in MeV; corresponding momenta are 573, 685 and 725 MeV/c

10. Abaev V.V. et al., Z. Phys. A - Atoms and Nuclei 322, 603 (1985).
11. Koch R., Z. Phys. C29, 597 (1985); Nucl. Phys. A448, 707 (986).
12. Sprung D.W.L., Phys. Rev. C32, 699 (1985).
13. Gersten A., Nucl. Phys. Rev. B12, 537 (1969).
14. Barrelet E., Nuovo Cimento A8, 331 (1972).
15. Abaev V.V., Kruglov S. P., Preprint PNPI 1794 (1992).
16. Davidson D. et al., Phys. Rev. D6, 1199 (1972); Carter A.A. et al., Nucl. Phys. B26, 445 (1971); Pedroni E. et al., Nucl. Phys. A300, 321 (1978).
17. Hohler G. et al., Preprint TKP 76/7, Karlsruhe University, 1976; Carter A. A. et al., Preprint RL-73-024, RPP/111, 1973.
18. Bugg D.V. et al., Nucl. Phys. B26, 588 (1971).
19. Bolochov A.A. et al., Preprint LNPI 750 (1982); 1491 (1989); World data compilation, LNPI Data Base.
20. Bussey P.J. et al., Nucl. Phys. B58, 363 (1973).
21. Sadler M. et al., Phys. Rev. D35, 2718 (1987); Phys. Lett. B119, 69 (1982).
22. Gordeev V.A. et al., Nucl. Phys. A364, 408 (1981); Preprint LNPI 209 (1979); 405 (1978).
23. Sadler, M., Proceedings of the Third International Symposium, Pion-Nucleon and Nucleon-Nucleon Physics, Gatchina, Vol. 1, p. 124 (1989); Supek I. et al., Phys. Rev. D47, 1762 (1993).
24. Abaev V.V. et al., Yad. Phys. 48, 5(11), 1338 (1988); Proc. of the 9th Int. Symp. on High Energy Spin Physics, Bonn, 1990, Springer-Verlag, 499 (1991).
25. Amsler C. et al., Lett. Nuovo Cimento 15, 209 (1976).

26. Amsler C. et al., Phys. Lett. B57, 289 (1975).
27. Bussey P.J., Thesis, Cambridge University, 1971.
28. Dubal L. et al., Helv. Phys. Acta 50, 815 (1977).
29. Roger E.H. et al., Rev. Mod. Phys. 33, 356 (1961).
30. Abaev V.V. et al., Z. Phys. A-Atoms and Nuclei 311, 217 (1983); Preprint LNPI 824 (1983); Bekrenev V. S. et al., Yad. Fiz. 24, 91 (1976); Nucl. Phys. A364, 515 (1981).
31. Mokhtari A. et al., Phys. Rev. D35, 810 (1987); Phys. Rev. D33, 296 (1986); Phys. Rev. Lett. 55, 359 (1985).
32. Gorn W. et al., LBL 1320, Berkeley, 1973; Bull. Am. Phys. Soc. 12, 469 (1967).
33. Ogden P.M. et al., Phys. Rev. B137, 1115 (1965).
34. Martin J.F. et al., Nucl. Phys. B89, 253 (1975).
35. Rothschild R.E. et al., Phys. Rev. D5, 499 (1972).
36. Bareyre P. et al., Phys. Rev. Lett. 14, 178, 878 (1965).
37. Sevior M.E. et al., Phys. Rev. C40, 2780 (1989).
38. Borcherding F.D., UCLA Thesis, 1982.
39. Jenefsky R.F. et al., Nucl. Phys. A290, 407 (1977).
40. Comiso J.C. et al., Phys. Rev. D12, 738 (1975).
41. Alder J.C. et al., Lett. Nuovo Cim. 23, 381 (1978).
42. Hauser M.J. et al., Phys. Lett. 35B, 252 (1971).
43. Kim G.J. et al., Phys. Lett. 219B, 62 (1989); Phys. Rev. D41, 733 (1990).
44. Hill R.E. et al., Phys. Rev. D2, 1199 (1970).
45. Arens J.F. et al., Phys. Rev. 167, 1261 (1968).
46. Berardo P.A. et al., Phys. Rev. D6, 756 (1972).
47. Chezc, J.B. et al., Nucl. Phys. B72, 365 (1974).
48. Kravtsov A.V. et al., Nucl. Phys. B140, 279 (1978).
49. Wightman J.A. et al., Phys. Rev. D38, 3365 (1988).
50. Brown R.M. et al., Nucl. Phys. B117, 12 (1976).
51. Brown R.M. et al., Nucl. Phys. B144, 287 (1978).
52. Debenham N.C. et al., Phys. Rev. D12, 738 (1975).
53. Chiu C.B. et al., Phys. Rev. 156, 1415 (1967).
54. Bulos F. et al., Phys. Rev. 187, 1827 (1969).
55. Sarma H.N.M. et al., Nucl. Phys. B161, 1 (1979).
56. Sarma H.N.M., Oxford University Thesis, 1976.
57. Eandy R.D. et al., Phys. Rev. 136, 536 (1964).
58. Richards T.J. et al., Phys. Rev., D10, 45 (1974).
59. Blasberg D.J. et al., UCLA-10-P25, 6 (1971).
60. Hyman E. et al., Phys. Rev. 165, 1437 (1968).
61. Seftor C.J. et al., Phys. Rev. D39, 2457 (1989).
62. Koch R. et al., Nucl. Phys. A336, 331 (1980).
63. Coudsmit P.F.A. et al., Nucl. Phys. A575, 673 (1994).
64. Gross F., Surya Y., Phys. Rev. C47, 703 (1993).
65. Pilkuhn H., "The Interaction of Hadrons", North-Holland, Amsterdam, 1967; "Relativistic Particle Physics", Moscow, Mir, 1983.
66. Birbrair B.L., Gridnev A. B., Preprint PNPI 1966 (1994).